

Origin of Oxide Sensitivity in Gold-Based Catalysts: A First Principle Study of CO Oxidation over Au Supported on Monoclinic and Tetragonal ZrO₂

Chuan-Ming Wang, Kang-Nian Fan, and Zhi-Pan Liu*

Contribution from the Shanghai Key Laboratory of Molecular Catalysis and Innovative Materials, Department of Chemistry, Fudan University, Shanghai 200433, China

Received October 20, 2006; E-mail: zpliu@fudan.edu.cn

Abstract: The catalytic performance of Au/oxide catalysts can vary significantly upon the change of oxide species or under different catalyst preparation conditions. Due to its complex nature, the physical origin of this phenomenon remains largely unknown. By extensive density functional theory calculations on a model system, CO oxidation on Au/ZrO₂, this work demonstrates that the oxidation reaction is very sensitive to the oxide structure. The surface structure variation due to the transformation of the oxide phase or the creation of structural defects (e.g., steps) can greatly enhance the activity. We show that CO oxidation on typical Au/ZrO₂ catalysts could be dominated by minority sites, such as monoclinic steps and tetragonal surfaces, the concentration of which is closely related to the size of oxide particle. Importantly, this variation in activity is difficult to understand following the traditional rules based on the O₂ adsorption ability and the oxide reducibility. Instead, electronic structure analyses allow us to rationalize the results and point toward a general measure for CO + O₂ activity, namely the p-bandwidth of O₂, with important implications for Au/oxide catalysis.

Introduction

Metal and metal oxide composites constitute some of the most important materials in heterogeneous catalysis.^{1–2} The oxide is traditionally regarded as the support merely for dispersing the active metal particles. Owing to the recent findings of the superior catalytic activity of Au/oxide systems,^{3–7} the oxide has demonstrated a vital role in catalysis since bare Au is never active enough.⁸ There has been considerable interest in the physical origin of the oxide-facilitated Au catalysis.^{9–17} By performing CO oxidation on clean Au surfaces,¹⁸ Au/TiO₂,^{19–23}

and Au/MgO,^{24,25} recent studies showed that (i) CO adsorbs at the low-coordinated sites of Au particles while O₂ adsorbs strongly at the Au/TiO₂ interface but weakly on pure Au and Au/MgO; (ii) CO oxidation can readily occur at the Au/TiO₂ interface. The O₂ adsorption was proposed to be the key step that influences the catalytic activity of Au/oxide catalysts.²⁶ This simple framework, however, met difficulties being extended to rationalize a large volume of experimental literature.^{27–32} Indeed, it remains unclear as to why the activity depends on the species and structure of the support. Obviously, a clear understanding of this important phenomenon is of huge importance toward designing and optimizing catalysts for emerging technology. Here, our efforts to rationalize the oxide-sensitivity phenomenon

- (1) Bell, A. T. *Science* **2003**, *299*, 1688.
- (2) Schlogl, R.; Abd Hamid, S. B. *Angew. Chem., Int. Ed.* **2004**, *43*, 1628.
- (3) Haruta, M.; Tsubota, S.; Kobayashi, T.; Kageyama, H.; Genet, M. J.; Delmon, B. *J. Catal.* **1993**, *144*, 175.
- (4) Haruta, M. *Catal. Today* **1997**, *36*, 153.
- (5) Chen, M. S.; Cai, Y.; Yan, Z.; Goodman, D. W. *J. Am. Chem. Soc.* **2006**, *128*, 6341.
- (6) Fu, Q.; Saltsburg, F.; Flytzani-Stephanopoulos, M. *Science* **2003**, *301*, 935.
- (7) Chen, M. S.; Goodman, D. W. *Science* **2004**, *306*, 252.
- (8) Hammer, B.; Norskov, J. K. *Nature* **1995**, *375*, 238.
- (9) Sanchez, A.; Abbet, S.; Heiz, U.; Schneider, W. D.; Hakkinen, H.; Barnett, R. N.; Landman, U. *J. Phys. Chem. A* **1999**, *103*, 9573.
- (10) Lopez, N.; Norskov, J. K. *J. Am. Chem. Soc.* **2002**, *124*, 11262.
- (11) Hakkinen, H.; Abbet, S.; Sanchez, A.; Heiz, U.; Landman, U. *Angew. Chem., Int. Ed.* **2003**, *42*, 1297.
- (12) Yoon, B.; Hakkinen, H.; Landman, M.; Worz, A. S.; Antonietti, J. M.; Abbet, S.; Judai, K.; Heiz, U. *Science* **2005**, *307*, 403.
- (13) van Bokhoven, J. A.; Louis, C.; Miller, J. T.; Tromp, M.; Safonova, O. V.; Glatzel, P. *Angew. Chem., Int. Ed.* **2006**, *45*, 4651.
- (14) Lemire, C.; Meyer, R.; Shaikhtudinov, S.; Freund, H. J. *Angew. Chem., Int. Ed.* **2004**, *43*, 118.
- (15) Kim, T. S.; Stiehl, J. D.; Reeves, C. T.; Meyer, R. J.; Mullins, C. B. *J. Am. Chem. Soc.* **2003**, *125*, 2018.
- (16) Guzman, J.; Gates, B. C. *J. Am. Chem. Soc.* **2004**, *126*, 2672.
- (17) Yan, Z.; Chinta, S.; Mohamed, A. A.; Fackler, J. P.; Goodman, D. W. *J. Am. Chem. Soc.* **2005**, *127*, 1604.
- (18) Liu, Z. P.; Hu, P.; Alavi, A. *J. Am. Chem. Soc.* **2002**, *124*, 14770.

- (19) Liu, Z. P.; Gong, X. Q.; Kohanoff, J.; Sanchez, C.; Hu, P. *Phys. Rev. Lett.* **2003**, *91*, 266102.
- (20) Stiehl, J. D.; Kim, T. S.; McClure, S. M.; Mullins, C. B. *J. Am. Chem. Soc.* **2004**, *126*, 1606.
- (21) Stiehl, J. D.; Kim, T. S.; McClure, S. M.; Mullins, C. B. *J. Am. Chem. Soc.* **2004**, *126*, 13574.
- (22) Molina, L. M.; Rasmussen, M. D.; Hammer, B. *J. Chem. Phys.* **2004**, *120*, 7673.
- (23) Liu, Z. P. *Phys. Rev. B* **2006**, *73*, 233410.
- (24) Molina, L. M.; Hammer, B. *Phys. Rev. Lett.* **2003**, *90*, 206102.
- (25) Molina, L. M.; Hammer, B. *Phys. Rev. B* **2004**, *69*, 155424.
- (26) Liu, L. M.; McAllister, B.; Ye, H. Q.; Hu, P. *J. Am. Chem. Soc.* **2006**, *128*, 4017.
- (27) Knell, A.; Barnickel, P.; Baiker, A.; Wokaun, A. *J. Catal.* **1992**, *137*, 306.
- (28) Grunwaldt, J. D.; Kiener, C.; Wogerbauer, C.; Baiker, A. *J. Catal.* **1999**, *181*, 223.
- (29) Comotti, M.; Li, W. C.; Spliethoff, B.; Schuth, F. *J. Am. Chem. Soc.* **2006**, *128*, 917.
- (30) Arrii, S.; Morfin, F.; Renouprez, A. J.; Rousset, J. L. *J. Am. Chem. Soc.* **2004**, *126*, 1199.
- (31) Zhang, X.; Wang, H.; Xu, B. Q. *J. Phys. Chem. B* **2005**, *109*, 9678.
- (32) Lomello-Tafin, M.; Chaou, A. A.; Morfin, F.; Caps, V.; Rousset, J. L. *Chem. Commun.* **2005**, 388.

at the atomic level are reported, and the reactant electronic properties are correlated to the activity.

Experimentally, the supporting oxides in Au/oxide catalysts are classified into two types, inert (e.g., MgO, SiO₂) and active (e.g., TiO₂, Fe₂O₃, IrO₂).^{33,34} The Au/active materials usually exhibit much higher activity than the Au/inert materials for CO oxidation. The active oxides are often reducible, e.g., TiO₂, while the inert oxides are usually irreducible insulators such as MgO. It was therefore suspected that the reducibility of the oxide makes the difference. However, this suggestion was questioned recently, as new experiments showed that Au supported on Al₂O₃ or ZrO₂ (irreducible oxides) can be quite active for CO oxidation, whereas Au supported on ZnO (reducible oxide) may perform poorly.^{29,30} This inconsistency was thought to be caused by different catalyst preparation methods. For example, for Au supported on the irreducible oxide ZrO₂, a number of experiments have reported a significant variation in activity for CO oxidation.^{27–32} Grunwaldt et al. found that the Au/TiO₂ catalyst showed significantly higher activity than the Au/ZrO₂ catalyst.²⁸ Using the colloidal deposition methods, Comotti et al. clearly indicated that ZrO₂ is substantially less active than TiO₂ support.²⁹ However, using laser evaporation, Arrii and coauthors synthesized ZrO₂- and TiO₂-supported Au model catalysts. They found that TiO₂ is slightly better than ZrO₂ as support, and the TOF of Au/TiO₂ (1.1 s⁻¹) is only 4 times larger than that of Au/ZrO₂ (0.28 s⁻¹).³⁰ Furthermore, the size of the oxide particles was found to be critical to the activity. Zhang et al. showed that Au supported on ZrO₂ nanoparticles (5–15 nm) can yield about 1 order of magnitude higher activity than that of Au supported on the larger ZrO₂ particles (40–200 nm).³¹ All these new experimental findings implied that certain, as yet undetermined, fundamental properties of the oxide are vital to activity.

Aiming to build a complete framework for Au/oxide catalysis, in this work CO oxidation over Au supported on various ZrO₂ surfaces (Au/ZrO₂) is investigated using first principles density functional theory (DFT) calculations. Our results provide a detailed dataset to compare with previous theoretical results on Au/TiO₂ and Au/MgO systems.^{19,24} Although the previous surface science studies indicated that oxygen vacancies on the support (such as the F center on MgO) may increase the activity of the Au/oxide catalysts dramatically due to the charging effect of Au,^{9,11,12} this work is concerned with nearly neutral Au particles on differently structured oxide surfaces, which should be more relevant to “real catalysts” prepared by typical chemical methods. With several ZrO₂ surfaces being considered as substrates, including two crystal phases and their structural defects, the oxide structure sensitivity in Au/ZrO₂ catalysis is identified and rationalized. Such oxide structure effects could be common to oxide-supported metal catalysts and thus is of general interest to chemistry.

Computational Method and Model

All DFT slab calculations were performed using the SIESTA package with numerical atomic orbital basis sets and Troullier–Martins norm-conserving pseudopotentials.^{35–37} The exchange–correlation functional

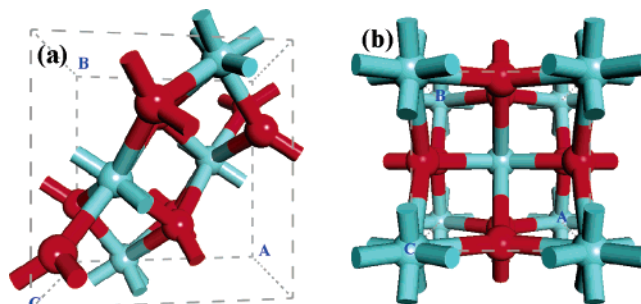


Figure 1. Crystal structures of (a) the monoclinic ZrO₂ and (b) the tetragonal ZrO₂. The red and cyan balls represent O and Zr atoms, respectively.

used was the generalized gradient approximation method, known as GGA-PBE.³⁸ A double- ζ plus polarization basis (DZP) set was employed. The orbital-confining cutoff radii were determined from an energy shift of 0.01 eV. The energy cutoff for the real space grid used to represent the density was set as 150 Ry. To further speed up calculations, the Kohn–Sham equation was solved by an iterative parallel diagonalization method that utilizes the ScaLAPACK subroutine pdsygvx with two-dimensional block cyclicly distributed matrix.³⁹ The Broyden method was employed for geometry relaxation until the maximal forces on each relaxed atom was less than 0.1 eV/Å. Transition states (TSs) of the catalytic reactions were searched using the constrained minimization method, where the Broyden method was employed to relax all the degrees of freedom except for the constrained reaction coordinate.^{40,41} The TSs are identified when (i) the forces on the atoms vanish and (ii) the energy is a maximum along the reaction coordinate, but a minimum with respect to all of the other degrees of freedom.

To pinpoint the active site in composite catalysts is a great challenge to both experiment and theory. It is well-known that synthesized ZrO₂ is often a mixture of two phases, monoclinic (m-ZrO₂, *P21/c* symmetry) and tetragonal phases (t-ZrO₂, *P42/nmc* symmetry) (see Figure 1).⁴² m-ZrO₂ is a more stable phase than t-ZrO₂, whereas the t-ZrO₂ phase is more populated with small zirconia particles.³¹ Therefore, we anticipated addressing the activity of Au/ZrO₂, both phases together with their defects having to be taken into account. Four different low-Miller-index surfaces were selected as substrates, namely, the flat ZrO₂ surfaces m-ZrO₂{ $\bar{1}11$ } and t-ZrO₂{101}, and the stepped surfaces m-ZrO₂{ $\bar{2}12$ } and t-ZrO₂{302}. The two flat surfaces are the most stable surface planes in each phase, respectively. m-ZrO₂{ $\bar{2}12$ } contains m-ZrO₂{ $\bar{1}01$ } steps and m-ZrO₂{ $\bar{1}11$ } terraces, while t-ZrO₂{302} is constituted by t-ZrO₂{100} steps and t-ZrO₂{101} terraces. As the stepped m-ZrO₂{ $\bar{1}01$ } and t-ZrO₂{100} are the second-lowest surface energy planes in each phase, respectively, these types of steps should be the most common structural defects in ZrO₂ particles.⁴³ Both oxides are insulating. The calculated band gaps are 3.41 eV (exp 4.2 eV) and 3.86 eV (exp 4.2 eV) for m-ZrO₂ and t-ZrO₂ oxide, respectively, which are in good agreement with previous theoretical results with plane-wave methods.^{44,45}

The Au/ZrO₂ systems were then modeled by adding a two-layer strip of Au on the top of the stoichiometric oxide surfaces (see Figure 2). Similar methods have been successfully applied to study the catalytic

(33) Schubert, M. M.; Hackenberg, S.; vanVeen, A. C.; Muhler, M.; Plzak V.; Behm R. J. *J. Catal.* **2001**, *197*, 113.

(34) Liu, Z. P.; Jenkins, S. J.; King, D. A. *Phys. Rev. Lett.* **2004**, *93*, 156102.

(35) Soler, J. M.; Artacho, E.; Gale, J. D.; Garcia, A.; Junquera, J.; Ordejon, P.; Sanchez-Portal, D. *J. Phys.: Condens. Matter* **2002**, *14*, 2745.

(36) Junquera, J.; Paz, O.; Sanchez-Portal, D.; Artacho, E. *Phys. Rev. B* **2001**, *64*, 235111.

(37) Troullier, N.; Martins, J. L. *Phys. Rev. B* **1991**, *43*, 1993.

(38) Perdew, J. P.; Burke, K.; Ernzerhof, M. *Phys. Rev. Lett.* **1996**, *77*, 3865.

(39) http://www.netlib.org/scalapack/scalapack_home.html.

(40) Liu, Z. P.; Jenkins, S. J.; King, D. A. *J. Am. Chem. Soc.* **2004**, *126*, 10746.

(41) Liu, Z. P.; Hu, P. *J. Am. Chem. Soc.* **2003**, *125*, 1958.

(42) Christensen, A.; Carter, E. A. *Phys. Rev. B* **1998**, *58*, 8050.

(43) Liu, Z. P.; Wang, C. M.; Fan, K. N. *Angew. Chem., Int. Ed.* **2006**, *46*, 6865.

(44) Jomard, G.; Petit, T.; Pasturel, A.; Magaud, L.; Kresse, G.; Hafner, J. *Phys. Rev. B* **1999**, *59*, 4044.

(45) McComb, D. W. *Phys. Rev. B* **1996**, *54*, 7094.

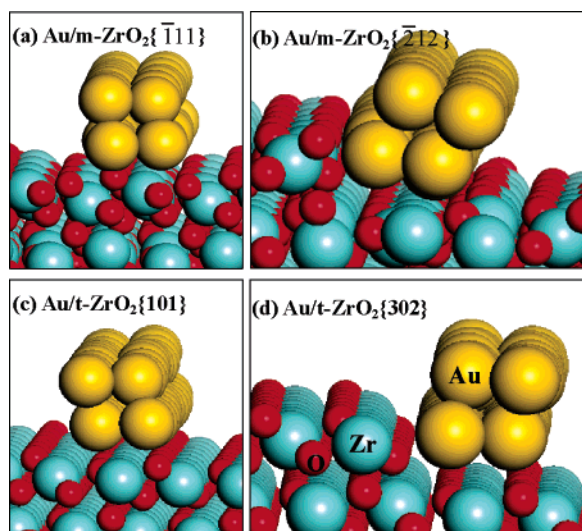


Figure 2. Optimized structures for the Au strip on the four different ZrO₂ surfaces. The red, cyan, and yellow balls represent O, Zr, and Au atoms, respectively.

Table 1. Adsorption Energy $E_{\text{ad}}(\text{O}_2)$, the Bond Distance $d_{\text{O-O}}$, and the Mulliken Charge $\Delta Q(\text{O}_2)$ of O₂ Adsorbed at the Au/ZrO₂ Interfaces; Change of Mulliken Charge of Au Strip $\Delta Q(\text{Au})$ and the Support ZrO₂ $\Delta Q(\text{ZrO}_2)$ after the Adsorption of O₂ are Also Listed

	$E_{\text{ad}}(\text{O}_2)/$ eV	$d_{\text{O-O}}/$ Å	$\Delta Q(\text{O}_2)/$ e	$\Delta Q(\text{Au})/$ e	$\Delta Q(\text{ZrO}_2)/$ e
Au/m-ZrO ₂ {111}	0.88	1.475	-0.79	+0.70	+0.09
Au/m-ZrO ₂ {212}	1.07	1.445	-0.68	+0.63	+0.05
Au/t-ZrO ₂ {101}	1.08	1.485	-0.79	+0.76	+0.03
Au/t-ZrO ₂ {302}	1.71	1.475	-0.77	+0.87	-0.10

activity of Au/TiO₂.¹⁹ It should be mentioned that the two-layer strip of Au is a reasonable and realistic model based on previous findings: (i) Experiment showed that two-layers of Au particles on TiO₂ are the most effective arrangement for catalyzing CO oxidation.⁵ (ii) Theoretically, it was confirmed that appreciable CO and O₂ adsorption is observed only at the low coordinated Au atoms.¹⁸ In the study of CO oxidation on Au/TiO₂,^{19,22} and Au/MgO,^{24,25} it was found that the most feasible pathway for the reaction involves CO adsorption at the step-edge of the second-layer Au and O₂ adsorption at the Au/oxide interface. Thus, a two-layer model is sufficient to capture the important chemistry occurring at the interface.

The Au/ZrO₂ structures were initially relaxed using Nose thermostat molecular dynamics at 200 K for ~1000 fs, which is essential to locate the best geometry for the Au strip on the substrate. The lattice match between the optimized Au strip and the supporting oxide is generally good, being within ~1% mismatch. This is mainly due to the large unit cell of substrate surfaces utilized: m-ZrO₂{111} [p(2 × 2), 13.63 Å × 14.75 Å], t-ZrO₂{101} [p(3 × 4), 19.19 Å × 14.48 Å], m-ZrO₂{212} [p(3 × 1), 20.44 Å × 11.69 Å], and t-ZrO₂{302} [p(1 × 4), 17.40 Å × 14.48 Å]. Because of the large unit cell used and the insulating oxide support, only the Γ -point was used to sample the Brillouin zone in our calculations. The convergence of adsorption energy and reaction barrier with respect to k -point sampling has further been checked by utilizing (2 × 2 × 1) k -point set (the difference is found to be within 0.1 eV). Other calculation details are as those described in the previous work,¹⁹ where the accuracy of the SIESTA method was carefully benchmarked with a plane-wave methodology.

Results and Discussion

Figure 2 shows the optimized structures of the Au strip on the four different ZrO₂ surfaces. The optimized Au structures exhibit close-packed, (111)-like facets. In general, the Au strip

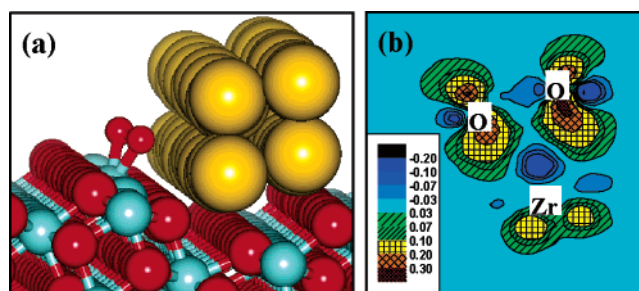


Figure 3. (a) Optimized structure, and (b) the charge density difference ($\text{e}/\text{\AA}^3$) plot showing the Zr–O₂ bonding plane of the O₂ adsorption on Au/t-ZrO₂{302}.

anchors on ZrO₂ through the lattice oxygens. The Au strip adsorption energy is defined as $E_{\text{ad}}(\text{Au}) = -(E_{\text{Au/oxide}} - E_{\text{oxide}} - E_{\text{Au}})/N_{\text{first-Au}}$, where E_X is the DFT total energy of the system X; $N_{\text{first-Au}}$ is the number of the first-layer Au atoms that are in close contact with the oxide. From our calculations, $E_{\text{ad}}(\text{Au})$ is around 0.20 eV for Au/m-ZrO₂{111}, Au/t-ZrO₂{101}, and Au/t-ZrO₂{302} and 0.26 eV for Au/m-ZrO₂{212}. This indicates that the Au strips bind weakly on ZrO₂, in analogy to Au on stoichiometric TiO₂¹⁹ and MgO⁴⁶ surfaces. The slightly larger adsorption energy of Au on m-ZrO₂{212} may be attributed to more two-fold oxygens exposed at step-edges.

Subsequently, O₂ on Au/ZrO₂ was examined by exploring O₂ adsorption on Au, ZrO₂, and their interfaces. O₂ adsorption energy is defined as $E_{\text{ad}}(\text{O}_2) = -[E(\text{O}_2/\text{Au/ZrO}_2) - E(\text{Au/ZrO}_2) - E(\text{O}_2)]$. As expected, the most stable adsorption configuration for O₂ is at the Au/ZrO₂ interface. The adsorption energy, the bond distance O–O, and the Mulliken charge of the adsorbed O₂ molecule are listed in Table 1. It can be seen that the O₂ adsorption energy is 0.88 eV at the Au/m-ZrO₂{111} interface, and it increases to 1.07 and 1.08 eV at the Au/m-ZrO₂{212} and Au/t-ZrO₂{101} interfaces, respectively. At the Au/t-ZrO₂{302} O₂ adsorbs remarkably strongly with an adsorption energy of 1.71 eV (the structure is shown in Figure 3a).⁴⁷ The Mulliken charge on the adsorbed O₂ range from -0.68 |e| to -0.79 |e| at the interfaces (Table 1). Because the large electron accumulation destroys the degeneracy of the O₂ 2 π^* states, the adsorbed O₂ at the interface is spin unpolarized, with a O–O bond length of over 1.40 Å (the gas-phase O₂ distance is 1.24 Å from DFT). This is similar to O₂ adsorption at the Au/rutile-TiO₂{110} interface, where the adsorption energy is calculated to be 0.86 eV.¹⁹

From Mulliken charge analysis (Table 1), it is clear that the electron accumulation on O₂ is mainly due to the electron depletion on Au, while the total charge of the ZrO₂ support is perturbed marginally by the presence of O₂. This may be better viewed from the calculated charge density difference plot in Figure 3b. The plot represents the charge density change that occurs when the gas-phase O₂ is brought onto the Au/t-ZrO₂{302} (O₂ adsorption on other systems is similar and thus not shown). The charge density difference is defined as: $\rho(\text{O}_2/\text{Au/ZrO}_2) - \rho(\text{O}_2) - \rho(\text{Au/ZrO}_2)$, where $\rho(\text{O}_2/\text{Au/ZrO}_2)$, $\rho(\text{O}_2)$, and $\rho(\text{Au/ZrO}_2)$ are the total charge densities of O₂/Au/ZrO₂, a free O₂ molecule, and Au/ZrO₂ systems without changing their atomic positions. This difference is positive in the regions where

(46) Ricci, D.; Bongiorno, A.; Pacchioni, G.; Landman, U. *Phys. Rev. Lett.* **2006**, *97*, 036106.

(47) It may be borne in mind that the O₂ adsorption energy on metal systems is generally overestimated by DFT (See refs 50, 51).

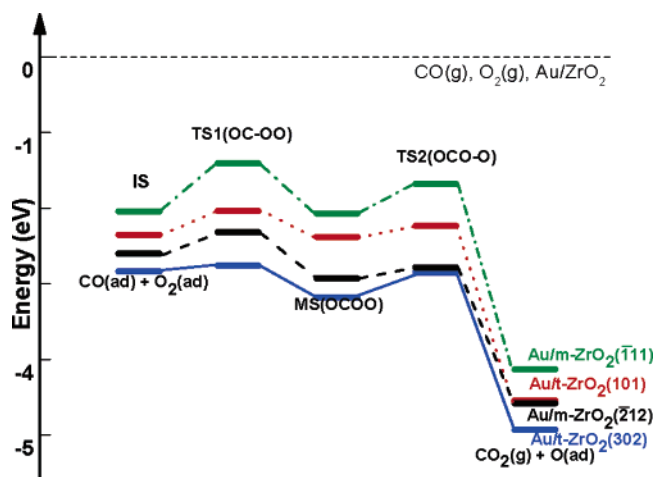


Figure 4. Energy profiles for CO oxidation over Au on four different ZrO₂ surfaces.

Table 2. Reaction Barriers for CO + O₂ → OCOO (E_a^1), and OCOO → CO₂ + O (E_a^2) Steps at Au/Oxide Interfaces, Respectively

oxide	m-ZrO ₂ {111}	m-ZrO ₂ {212}	t-ZrO ₂ {101}	t-ZrO ₂ {302}
E_a^1	0.63	0.28	0.32	0.08
E_a^2	0.39	0.15	0.23	0.33
$W_{p\text{-band}}^a$	13.47	12.94	12.93	12.14

^a $W_{p\text{-band}}$ is the calculated O₂ p-bandwidth (see text for definition). The units are eV.

the electronic charge accumulates upon adsorption, and negative where the charge depletes. It is obvious that upon adsorption electrons accumulate on the O₂ 2π* orbitals. The electron density on Zr is highly polarized to maximize the electrostatic interaction between the negative O₂ and the Zr cation.

Interestingly, our results show that the reducibility of the supporting oxide is not necessarily connected to its ability to promote O₂ adsorption. As an irreducible oxide, ZrO₂ performs very well to facilitate O₂ adsorption, comparable to the Au/TiO₂ interface (0.86 eV).¹⁹ By contrast, the irreducible oxide MgO is a poor support since the calculated O₂ adsorption energy at the Au/MgO interface (~0.2 eV)^{24,25} is not far from O₂ at the bare Au (~0.0 eV).¹⁸

We now consider CO oxidation at the Au/ZrO₂ interface. There are apparently two types of mechanisms: (i) CO reacts directly with molecular O₂, and (ii) O₂ dissociates first and CO then reacts with atomic O. Since our calculated O₂ dissociation barriers at the Au/ZrO₂ interface (O₂ → 2O) are generally higher than the corresponding CO + O₂ reaction barriers, the atomic oxygen reaction mechanism, i.e., O₂ → 2O; CO + O → CO₂, is not the lowest-energy pathway and thus not considered here. The reaction profiles for CO oxidation over four different Au/ZrO₂ interfaces are shown in Figure 4, the reaction barriers are listed in Table 2, and the geometrical structures of the initial state, transition states, and intermediate state are displayed in Figure 5.

As shown, CO initially adsorbs at the edge of the second Au layer in all cases. CO can then react with the interface O₂ through a bimolecular transition state (OC–OO). After the transition state, a metastable OCOO complex is formed.^{22,24} The OCOO complex exhibits a coplanar structure with its C end (from CO) attaching to Au and the O end (from O₂) sitting on Zr. Its internal O–O bond can then break, leading to the

formation of a CO₂ and an O adatom at the interface. The O adatom can easily be removed by adsorbed CO (the reaction barrier is very low, ~0.05 eV).

Among the elementary reaction steps, the CO + O₂ → OCOO step involves two molecules, in which the position of O₂ adsorption and the direction that CO attacks O₂ are all related to the detailed substrate structure. It is expected that the energy barriers of the CO + O₂ → OCOO step are more substrate sensitive. This is indeed confirmed by the strong variation in barrier E_a^1 , ranging from 0.08 to 0.63 eV. On the other hand, the dissociation of OCOO intermediate is less sensitive to the oxide structure, and the barrier E_a^2 differs no more than 0.2 eV from one surface to another. Therefore, the key to enhance CO oxidation activity is to reduce the reaction barrier E_a^1 of the first reaction step. It is also interesting to notice that as the intermediates during CO oxidation become more stable (Figure 4), the difference of E_a^1 and E_a^2 ($E_a^1 - E_a^2$) changes gradually from positive ($E_a^1 > E_a^2$) to negative ($E_a^1 < E_a^2$). Consequently, the rate-determining step of CO oxidation is expected to switch from the OCOO formation step to the OCOO decomposition step. This is in fact understandable from the basis of the concept of catalysis, known as Sabatier principle: the optimum activity is the compromise between the rate and strength of chemisorption. If the reaction intermediates are too weakly bonded on the surface, the first step (typically dissociation of reactants) would be too slow to occur; however, if the reaction intermediates are too tightly bonded on the surface, the desorption of products (typically recombination reactions) would be rate limiting. This phenomenon has recently been well addressed by Norskov et al. in ammonia synthesis.⁴⁸

By comparing the reaction barriers for CO oxidation on the surfaces, one can conclude that the monoclinic stepped surface with the highest barrier being only 0.28 eV is the best catalyst among all the surfaces considered. Our results indicate that CO oxidation on Au/ZrO₂ may be dominated by a small number of stepped sites of monoclinic ZrO₂ considering that the monoclinic phase is the most stable phase of ZrO₂. According to the rate equation TOF = $k e^{-E_a/RT}$ [sites], the reaction rate of the CO + O₂ reaction at the stepped sites (room temperature) are at least 3 orders of magnitude larger than that at the flat surfaces, assuming the concentration of stepped sites is only 1% of that of the flat surface sites and the pre-exponential factors k are identical. In addition, the presence of the less stable tetragonal phases can also enhance the activity since the barriers of CO oxidation at Au/t-ZrO₂ interfaces are also much lower than those at Au/m-ZrO₂{111}. With the higher activity at the stepped monoclinic surfaces and at the tetragonal phase, the rate of CO oxidation is expected to increase with the decrease of ZrO₂ particle size since small ZrO₂ particles will expose more structural defects and also contain a higher concentration of tetragonal phases. This supports the experimental findings,³¹ in which Zhang et al. suggested that it is the increase of Au/oxide boundary populations which enhances CO oxidation activity.³¹ Our results here provide an explanation from the atomic level, emphasizing the critical role of minority sites, i.e., stepped m-ZrO₂ and t-ZrO₂ surfaces.

To shed light on the relationship between oxide structure and activity, we have first calculated the d-projected density of states

(48) Bligaard, T.; Norskov, J. K.; Dahl, S.; Matthiesen, J.; Christensen, C. H.; Sehested, J. *J. Catal.* **2004**, *224*, 206.

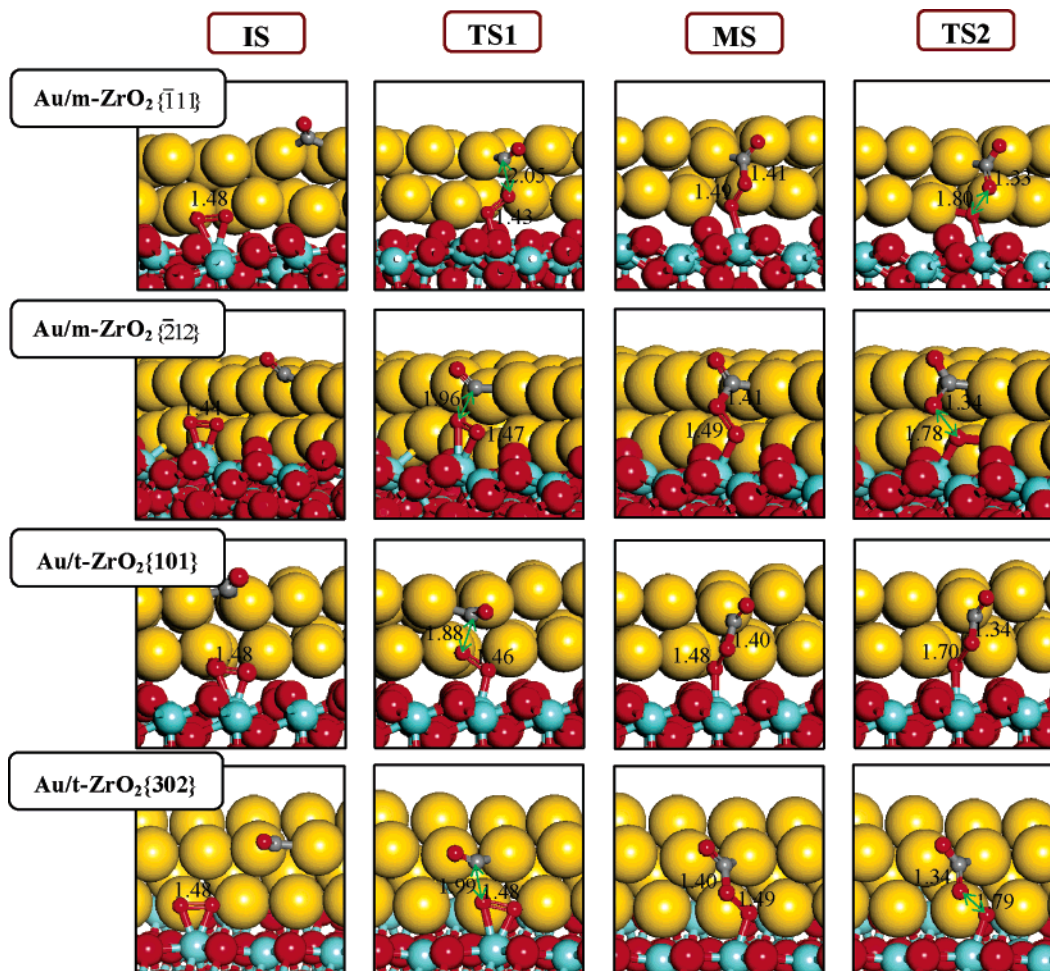


Figure 5. Optimized structures of the initial- (IS), transition- (TS1 and TS2), and intermediate-states (MS) for CO oxidation at four different Au/ZrO₂ interfaces.

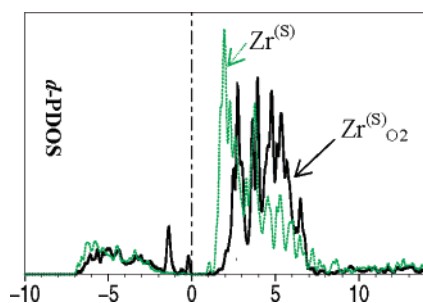


Figure 6. d-Projected density of states of Zr atoms in the O₂/Au/t-ZrO₂-{302} system. The Fermi level is set as energy zero.

of the surface Zr atoms in the O₂ adsorbed Au/ZrO₂ systems. In each system, the surface Zr bonded with the O₂ (labeled as Zr^(s)O₂) is selected for analysis to compare with a reference Zr atom that is a normal surface Zr atom (labeled as Zr^(s)). For illustration, the Zr d-PDOSs of the Au/t-ZrO₂{302} surface are plotted in Figure 6. It shows that most Zr d states are located in the unoccupied conduction band; due to the extra bonding with O₂, the d states of Zr^(s)O₂ is upshifted in energy compared to the d states of Zr^(s). In the d-PDOS of Zr^(s)O₂ there are few extra small peaks around the Fermi level, which are found to be the mixing states between the d-Zr^(s)O₂ and the O₂ 2π* orbitals. Combining Figure 3b and Figure 6, we can see that the Zr–O₂ interaction through the 4d(Zr) – 2π*(O₂) mixing possesses clear covalent bonding characteristics. Because the d

states of Zr are largely empty before and after O₂ adsorption, the electron density difference plot (Figure 3b) does not reveal the rehybridization in the d-orbitals. Nevertheless, the energy change of the Zr d states (E_d) can be quantitatively evaluated by

$$E_d = \int_{-\infty}^{+\infty} \epsilon \cdot (n_d^{O_2\text{-ad}} - n_d^{\text{bare}}) d\epsilon \quad (1)$$

where n_d are the normalized density of states of Zr (unit: electron/eV) with and without O₂ bonding; ϵ is the energy level (eigenvalue). The calculated E_d is 2.72, 5.88 eV for t-ZrO₂ flat and stepped surfaces, while it is 1.26 and 1.80 eV for m-ZrO₂ flat and stepped surfaces, respectively. For comparison, E_d for the surface Ti atom in the O₂/Au/TiO₂ system is also calculated, which is 2.83 eV. As E_d varies significantly from system to system, it is a qualitative representation of the local activity of metal cation d states. The larger E_d indicates the more active d states, and vice versa.

From the calculated E_d , we can see that compared to the monoclinic phase Zr, the tetragonal phase Zr cations can interact more strongly with O₂ and are thus more active. This may not be surprising as t-ZrO₂ is a less stable phase than m-ZrO₂ (the calculated cohesive energy of t-ZrO₂ is 0.11 eV per ZrO₂-unit less than m-ZrO₂). Also obvious is that the step-edge Zr cations with generally large E_d are more active than the flat surface Zr cations. These two trends qualitatively coincide with the

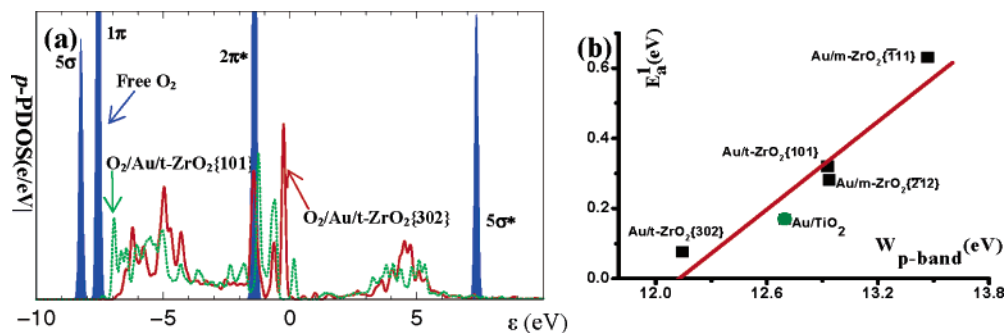


Figure 7. (a) p-Projected density of states for adsorbed O₂ at Au/t-ZrO₂{302} and Au/t-ZrO₂{101} (*p*-PDOS of a free O₂ molecule (spin-unpolarized) is also shown for comparison), and (b) the plot of CO + O₂ reaction barrier (E_a^1) against *p*-bandwidth of O₂.

determined CO + O₂ activity (E_a^1) in the Au/ZrO₂ systems. The important role of d states in activating O₂ may also be extended to understand the high activity of TiO₂ and the low activity of MgO. For Au/TiO₂, the $E_d(\text{Ti})$ (2.83 eV) of the flat rutile-TiO₂{110} is quite large, indicating a strong local interaction between O₂ and Ti. In MgO systems, by contrast, where the d states are not available, O₂ is not activated enough, as evidenced by its very low adsorption energy. It should be mentioned that some system-dependent effects such as surface relaxation after O₂ adsorption also contribute significantly to E_d (e.g., upon O₂ adsorption the existing O–Zr bond will undergo relaxation). This disfavors E_d as a direct measure for the activity of O₂.

Alternatively, we have analyzed the *p* states of adsorbed O₂, as illustrated in Figure 7a. Similar to its gas-phase counterpart, the *p*-projected density of states (*p*-PDOS) of an adsorbed O₂ constitutes three main regions: (a) O₂-bonding region (mainly 5σ and 1π) from –7.5 to –3 eV; (b) O₂ 2π* antibonding region from –3 to +0.5 eV; (c) O₂ 2π* and 5σ* antibonding region: from +0.5 to +7 eV. From the *p*-PDOSs, two obvious features of adsorbed O₂ can be singled out as compared to that of a free O₂: first, the broadening of individual O₂ molecular states and, second, the decreased width of the whole *p*-band. The first feature is universal for molecules interacting with solid surfaces as predicted by the News–Anderson model.⁴⁹ The second can also be explained by considering the O₂ bond weakening upon adsorption, which reduces the energy splitting between its bonding (e.g., 5σ) and antibonding states (e.g., 5σ*).

On finding this, we have tentatively plotted the calculated CO + O₂ reaction barrier (E_a^1) against the O₂ *p*-bandwidth ($W_{p\text{-band}}$) in Figure 7b. $W_{p\text{-band}}$ is defined as $W_{p\text{-band}} = \epsilon_C^{5\sigma^*} - \epsilon_C^{5\sigma}$, i.e. the energy difference between the band centers (ϵ_C) for O₂ 5σ and 5σ* states. The ϵ_C can be approximately calculated using eq 2

$$N_{\text{el}} = \int_{-\infty}^{\epsilon_C} n(\epsilon) d\epsilon \quad (2)$$

at $N_{\text{el}} = 0.5$ (for $\epsilon_C^{5\sigma}$) and $N_{\text{el}} = 11.5$ (for $\epsilon_C^{5\sigma^*}$), where $n(\epsilon)$ is the normalized *p*-PDOS of O₂ (i.e., $N_{\text{el}} = 12$ as $\epsilon \rightarrow +\infty$). As shown, the reaction barrier height, including that of Au/TiO₂ system ($W_{p\text{-band}}$ for O₂/Au/TiO₂ is 12.70 eV), can be correlated quite nicely with $W_{p\text{-band}}$. This implies that it is possible to

predict the catalytic activity by evaluating simply the electronic structure of reactants, i.e., the adsorbed O₂.

It should be pointed out that, in CO oxidation on Au/oxide systems (including ZrO₂, TiO₂), as CO adsorbs on the Au particles invariably, it may not then be surprising that the effect of CO is relatively unimportant, which leads to our observation that E_a^1 can be simplified as a function of an O₂ electronic property. We also noticed that the calculated O₂ distances at the interfaces are rather similar (~1.4 Å, see Figure 5) and thus apparently show no correlation with the calculated E_a^1 . This indicates that a subtle change in the electronic structure of O₂ will shift the reaction barrier considerably but has little effect on the adsorption geometry.

Our electronic structure analyses highlight the vital roles of the empty d-states of the metal oxide substrate in activating O₂. Although the d-states in oxides are largely unoccupied, they are able to mix with the low-lying O₂ 2π* orbitals to further lower the O₂ 2π* energy level, which subsequently leads to the electron flow from the Au strip to the O₂. The resulted *p*-bandwidth of O₂ can then be used as a fingerprint of O₂ activity. By varying the oxide species and crystal phases, and by creating surface defects, the d-states of the metal oxide can be modified and consequently change the O₂ adsorption behavior at Au/oxide interfaces. This is therefore a possible reason why CO oxidation over Au-based catalysts is sensitive to the catalyst preparation conditions.

Conclusions

In summary, this work demonstrates that the oxide crystal phases and structural defects can significantly modify catalyst activity through reaction kinetics in oxide-supported Au catalysis. The activity of the metal cation empty states varies significantly upon the change of oxide species and structures, which consequently results in the observed oxide sensitivity. We find that the O₂ *p*-bandwidth can be used as a tool to quantitatively predict the Au/oxide activity, whereas the traditional rules for judging the Au/oxide activity such as the oxide reducibility and O₂ adsorption ability are not applicable.

Acknowledgment. We acknowledge NSF of China (20573023, 20433020, 20673024), Pujiang Plan, and NSF of Shanghai Sci. Tech. Committee (06PJ14011, 02DJ14023, 05DZ22313) for financial support, and Shanghai Supercomputing Center is thanked for computing time.

JA067510Z

(49) News, D. M. *Phys. Rev.* **1969**, *178*, 1123.

(50) Ge, Q. F.; Kose, R.; King, D. A. *Adv. Catal.* **2000**, *45*, 207.

(51) Varganov, S. A.; Olson, R. M.; Gordon, M. S.; Metiu, H. *J. Chem. Phys.* **2003**, *119*, 2531.